Food Chemistry: X 26 (2025) 102266

Contents lists available at ScienceDirect

Food Chemistry: X

journal homepage: www.sciencedirect.com/journal/food-chemistry-x

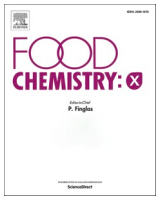

Effects of different crushing methods on the properties and flavor of selenium-enriched sweet potato leaves

Qi Gao [a,d,1], Jia-Nan Chen [a,b,1], Yu-Lu Tian [a,b], Miao-Miao Hao [a,b], Xuan-Li Sha [a,b], Ang Li [f], Xue Peng [a,b], Tao Yu [c,***], Xue-Jun Gu [e,**], You-Lin Xue [a,b,*]

[a] College of Light Industry, Liaoning University, Shenyang 110036, PR China
[b] Liaoning Key Laboratory of Food Bioprocessing, Shenyang 110036, PR China
[c] Tuber Division, Crop Research Institute, Liaoning Academy of Agricultural Sciences, Shenyang 110161, PR China
[d] Department of Regional Economic Development, Party School of Liaoning Provincial Party Committee, Shenyang 110161, PR China
[e] Institute of Rare and Scattered Elements, Liaoning University, Shenyang 110036, PR China
[f] Liaoning Institute of Standardization, Shenyang 110002, PR China

ARTICLE INFO

Keywords:
Se-enriched sweet potato leaves powder
Superfine grinding
Physicochemical property
Structural property
Flavor characteristic

ABSTRACT

In this study, the physical, chemical, structural, and antioxidant characteristics of selenium (Se)-enriched sweet potato leaves (SSPL) powder produced through shear breaking and superfine grinding were examined. The superfine grinding SSPL powder had a brighter color, smaller particle size, and spherical shape. The superfine grinding SSPL powder showed improved dispersibility and solubility but reduced liquidity. Superfine grinding destroyed the crystalline area and decreased the thermal stability, while Se application did not significantly change the ordered structure. Correlation analysis showed that superfine grinding could improve crude fiber, crude lipid, total flavonoids, total polyphenol, and significantly enhance the antioxidant activities compared to shear breaking. Se enrichment can enhance the content of the crude protein and the DPPH• scavenging activity and reducing power. The flavor characteristic was not altered with the different crushing methods and Se concentrations. SSPL powder could serve as a potential resource for a new solid beverage.

1. Introduction

Sweet potato (*Ipomoea batatas* L.) is one of the most important crops in China, after rice, wheat, and corn. China stands out as the leading producer of sweet potato, with yields reaching an impressive 7333 $ha{\cdot}hm^{-2}$ in 2021 (FAO, 2021). As one of the by-products of sweet potato, sweet potato leaves can be harvested multiple times during each cultivation period, offering higher returns than other leafy vegetables. They are natural nutritious and health-care vegetables that can lower cholesterol, improve human immunity, and prevent cardiovascular fat (Tang et al., 2021). However, it's important to note that the leaves are significantly underutilized, as only a tiny fraction of the resource is utilized as fresh produce for human consumption or animal feed. As a result, this inefficient resource utilization has also resulted in environmental pollution (Luo et al., 2021). The upcycling and utilization of sweet potato leaves will play a crucial role in enhancing the economic development of the sweet potato processing industry.

Selenium (Se) is a beneficial essential trace element and biologically active (anti-cancer and cardiovascular conditioning). Certain organic forms of Se, such as methylselenocysteine (MeSeCys), are believed to be highly effective sources of dietary Se (Dobrzyńska et al., 2023). It is renowned for its antioxidant, anti-inflammatory, chemopreventive,

Abbreviation: Se, Selenium; SSPL, Se-enriched sweet potato leaves.

* Corresponding author at: College of Light Industry, Liaoning University, No. 66 Chongshan Middle Road, Huanggu District, Shenyang, Liaoning Province, PR China.
** Corresponding author at: Institute of Rare and Scattered Elements, Liaoning University, No. 66 Chongshan Middle Road, Huanggu District, Shenyang, Liaoning, Province, PR China.
*** Corresponding author at: Tuber Division, Crop Research Institute, Liaoning Academy of Agricultural Sciences, No. 84 Dongling Road, Shenhe District, Shenyang, Liaoning, Province, PR China.
E-mail addresses: taoyu@cau.edu.cn (T. Yu), guxuejun@lnu.edu.cn (X.-J. Gu), xueyoulin@lnu.edu.cn (Y.-L. Xue).
[1] Qi Gao and Jia-Nan Chen contributed equally to this work.

https://doi.org/10.1016/j.fochx.2025.102266
Received 23 December 2024; Received in revised form 29 January 2025; Accepted 5 February 2025
Available online 5 February 2025

antiviral, and anticarcinogenic properties (Wang, Fang, et al., 2024). Low dietary Se intake can contribute to various health issues, such as heart disease, reduced male fertility, hypothyroidism, decreased immunity, increased susceptibility to disease, and elevated risk of cancer (Jia et al., 2023). It has been recognized that a moderate amount of Se can enhance the growth, nutrition, and sensory quality of crops. For example, the application of chelates Se significantly increased net photosynthesis and grain yield of fragrant rice (Hong et al., 2024). Biofortification with selenite (20 μg/g) in Golden needle mushrooms is effective in promoting the accumulation of nutrients, including polysaccharides, proteins, and iron (Dong et al., 2021). Moreover, Se application enhances the antioxidant defense system of Se-enriched sweet potato (SSP) stem. Consequently, SSP stem protein powder can be used as an antioxidant (Gao et al., 2021). For example, SSP stem protein powder may be used to process Chinese vermicelli. Furthermore, the use of Se can inhibit the uptake and storage of toxic metals in plants. For example, the $HgCl_2$ accumulation of lettuce was mitigated by foliar Se biofortification (Kavcic et al., 2020). Crops play a vital role in providing essential Se to humans and animals globally. Enhancing the Se content in food crops offers a promising solution to address the Se deficiency issue. Knowledge about the occurrence of Se and the course of its metabolic processes will allow the selection of food products that could be excellent ingredients in preventing Se deficiency in the diet in the future (Kieliszek & Sandoval, 2023).

Recently, the emulsifying capability of Se-enriched proteins has been reported. Protein fractions from germinated chickpeas in the presence of Se introduced excessive emulsifying capacity. Especially, glutelin protein fraction gathered the best Se content, emulsifying capacity, and confirmed up to 95 % mobile antioxidant ability (Hernández-Grijalva et al., 2022). The organic exercise and toxicity of Se are surprisingly related with its chemical species. Thus, more studies focused on the conversion of inorganic Se into organic forms (Wang, Yang, et al., 2024; Xiao et al., 2023). Notably, in the existing research on Se-enriched foods, the impact of the crushing method has been overlooked. Different crushing methods can change the physical properties of Se-enriched raw materials, such as particle size and specific surface area. However, the crushing method is one that may affect the stability of Se-containing compounds and the overall quality of Se-enriched foods. This remains an open question that requires in-depth research.

Superfine grinding technology is an advanced processing technique that can reduce materials to micrometer or even nanoscale powders. This technology significantly alters the structure and specific surface area of the powder, resulting in unique properties that are not found in ordinary particles, such as reduced syneresis and induced gelatinization (Dhiman & Prabhakar, 2021). At present, food industry has adopted a variety of crushing methods to make ready-to-eat powder products. Superfine grinding technology could improve the physicochemical properties of powder and was used in various plant powder processing, such as bilberry leaves (Jiang et al., 2017), moringa leaves (Huang et al., 2020), tobacco leaves (Zhang et al., 2021). It was also reported that the molecular weight and dissolution behavior of *Lycium barbarum* polysaccharides was changed by superfine grinding with enhanced antioxidant activity (Zhang et al., 2014). Furthermore, the concentration of extractable polyphenols in olive pomace significantly increased following the superfine grinding treatment. Additionally, barley seedlings (*Hordeum vulgare*) are made into ultra-fine barley leaf powder in Japan named barley green juice, which is rich in fiber, amino acids, vitamins, and trace elements. It can not only make up for the deficiency of daily vegetable intake to achieve balanced nutrition but also has a better healthcare effect of reducing fat, inhibiting cancer and antioxidation (Wang et al., 2022).

The objectives of this study were as follows: (a) To examine the absorption rate of Se in three by-products of sweet potato production: leaves, stems, and petioles. (b) To analyze how variations in Se concentrations affect the chemical composition, physicochemical properties, and flavor characteristics of Se-enriched sweet potato leaves (SSPL) powder. (c) To evaluate the impact of different crushing methods on the chemical composition, physicochemical properties, and flavor characteristics of SSPL powder.

2. Materials and methods

2.1. Materials

The plants of sweet potato were cultivated in Shenyang, Liaoning Province, China. During the planting period, manual weeding was carried out, and pesticides were not applied. During the growth of sweet potato plants, sodium selenite solutions at concentrations of 0, 0.5, 1.0, and 2.0 mg/L were sprayed onto the leaves three times, with each application consisting of 333 mL of the sodium selenite solution (Gao et al., 2019). The applications were done at intervals of approximately 20 d. The experimental setup included two columns of exploratory packages, with six for each line, and the bundles were divided by ditches around 30 cm. The disease-free fresh samples were collected and cleaned for further analysis when the sweet potatoes were harvested (Oct, 2022). Hydrochloric acid (HCl), and nitric acid (HNO_3) were purchased from Tianjin Yongda Chemical Reagent Co., Ltd. Sodium selenite, *V*c, Salicylic acid, pyrogallol ($C_6H_6O_3$) and potassium bromide (KBr) were purchased from Sinopharm Chemical Reagent Co., Ltd. 2,2-azino-bis(3-ethylbenzthiazoline-6-sulphonic acid) (ABTS) and 1,1′-diphenyl-2-picrylhydrazyl (DPPH) were obtained from Beijing Boao Tuoda Technology Co., Ltd.

2.2. Preparation of powder

The fresh SSPL was dried in a hot-air drying oven (GZX-9076MBE, BoXun Co., Ltd., Shanghai, China) for 72 h at 50 °C, and stored in a Ziplock bag until use. Dried SSPL was powdered by a universe high-speed pulverizer (SZ-500 A, Yongkang Co., Ltd., China), screened through a 100-mesh-sized sieve, and named shear breaking SSPL powder. Dried SSPL was also powdered by a planetary ball mill (DEC-PBM-V-0.4 L, Deco Equipment Co., Ltd., Changsha, China), screened through a 100-mesh-sized sieve, and named superfine grinding SSPL powder. The shear breaking SSPL powder samples were labeled as SB-Se0, SB-Se0.5, SB-Se1.0, and SB-Se2.0. The superfine grinding SSPL powder samples were labeled as SG-Se0, SG-Se0.5, SG-Se1.0, and SG-Se2.0. These categories corresponded to different Se concentrations for foliar application, including 0, 0.5, 1.0, and 2.0 mg/L sodium selenite.

2.3. Determination of chemical compositions

The Se contents of the samples were measured by the method of Gao et al. (2021) via dual-channel atomic fluorescence spectrometry (AFS-9800, Jitian Instrument Co., Ltd., Beijing, China). The standard curve was $Y = 37.66X - 442.74$ ($R^2 = 0.9999$). Total polyphenols and total flavonoids of SSPL powder were estimated by the method of Zhang et al. (2009). Using a nitrogen-to-protein conversion ratio of 6.25, the Kjeldahl distillation method was used to calculate the crude protein. Using petroleum ether as a solvent, the Soxhlet extraction method was used to assess the crude fat. Crude fiber was estimated based on the acid-base digestion method. Moisture was determined by the drying method. The ash content was estimated by heating to a constant weight in a muffle furnace at 650 °C.

2.4. Determination of color parameters

The color of the SSPL powder was assessed with a portable colorimeter (BYK 6801, BYK Instruments Co., Ltd., Shanghai, China). The color was presented as L* (lightness), a* (redness/greenness), and b* (yellowness/blueness). The overall color change (ΔE) of SSPL powder among samples was calculated using Eq. (1):

$$\Delta E = \sqrt{(L^* - L_0)^2 + (a^* - a_0)^2 + (b^* - b_0)^2} \quad (1)$$

where L_0, a_0, and b_0 were the color parameters of the control, L*, a*, and b* were the color parameters of other SSPL powder.

2.5. Determination of particle size

A laser diffraction particle size analyzer (Mastersizer 3000, Malvern Instrument Ltd., Worcestershire, UK) was used for the determination of the particle size of SSPL powder.

2.6. Analysis of flow properties

The angle of repose (θ) was determined using the method of Zhang et al. (2020). A funnel placed 3 cm above a testing platform received a continuous flow of SSPL powder. The measurement was considered complete when the formed cone made contact with the end of the funnel. The θ was calculated using Eq. (2) as described below:

$$\theta = arctan(H/R) \quad (2)$$

Where H (cm) represents the height of the powder cone, and R (cm) represents radius, respectively.

The angle of slide (α) was determined using the methodology detailed by Zhang et al. (2020). Three grams of SSPL powder was poured onto a glass surface and gradually tilted until the particles started to move together. The α was determined using Eq. (3) provided below:

$$\alpha = arcsin(H/L) \quad (3)$$

where H (cm) represents the vertical distance between the top of the inclined and horizontal planes, and L (cm) represents the length of the plane in centimeters, respectively.

The bulk density was calculated following the method described by Zhang et al. (2020). A measurement cylinder with a volume of 10 mL was filled with SSPL powder (M_1, approximately 2 g) and its volume (V_1) was then measured. The bulk density was determined using the formula provided in Eq. (4) below:

$$\rho_{bulk} = M_1/V_1 \quad (4)$$

Tap density was determined following the procedure outlined by Huang et al. (2020). An amount of SSPL powder was placed in a measuring cylinder and then agitated on a thick sponge until its volume no longer decreased. The tap density was determined using the Eq. (5) provided below:

$$\rho_{tap} = M_2/V_2 \quad (5)$$

where ρ_{tap}, V_2, and M_2 represent the tap density (g/mL), the measured volume (mL), and the weight of the powder (g), respectively.

2.7. Analysis of hydration properties

Following the approach outlined by Zhao et al. (2018), 0.5 g of SSPL powder (referred to as M_0) was combined with 50 mL of deionized water in centrifuge tubes (referred to as M_1), and placed in a refrigerator at 4 °C. After 24 h of settling, the supernatant was carefully removed after centrifugation, and the weight was recorded as M_2. The water holding capacity (WHC) was subsequently determined using the Eq. (6) provided below:

$$WHC\ (g/g) = (M_2 - M_1 - M_0)/M_0 \quad (6)$$

Following the approach outlined by Huang et al. (2021), 0.5 g of SSPL powder (M_0) was mixed with 10 mL of peanut oil in centrifuge tubes (M_1) using a vortex mixer (XH-C, Xinbao Instruments Ltd., Jiangsu, China). The mixture was allowed to sit for 1 h and then centrifuged at 3100 ×*g* for 30 min. The supernatant was then removed using a pipette, and the tubes containing the powder (M_2) were weighed again. The oil holding capacity (OHC) was determined using the Eq. (7) provided below:

$$OHC\ (g/g) = (M_2 - M_1 - M_0)/M_0 \quad (7)$$

Freeze-thaw stability (FTS) was assessed following the procedure outlined by Yu et al. (2018). In a centrifuge tube labeled M1, 1 *g* of SSPL powder was combined with 15 mL of deionized water, stirred for 30 min at 30 °C, then refrigerated at 20 °C for 24 h. The sample was then thawed, and centrifuged in a new tube labeled M_2, the supernatant was discarded, and the remaining content was weighed (M_3). The freeze-thaw stability (FTS) was determined using the Eq. (8) provided below:

$$FTS\ (g/g) = (M_2 - M_3)/(M_2 - M_1) \quad (8)$$

Water swelling capacity (WSC) was measured following the method described by Zhang et al. (2009). Initially, the weight (M) of SSPL powder was measured and placed into a 15 mL graduated cylinder. Subsequently, the initial volume (V_1) of the dried powder was recorded. Next, 10 mL of distilled water was added to the graduated cylinder containing the powder and mixed thoroughly. The cylinder was then shaken well and left undisturbed at 25 °C for 24 h. After the designated time, the final volume (V_2) of the swollen powder was measured. The water swelling capacity (WSC) was determined using the Eq. (9) as provided below:

$$WSC\ (mL/g) = (V_2 - V_1)/M \quad (9)$$

The water solubility index (WSI) was measured following the method described by He et al. (2019). SSPL powder (W_1, g) was dissolved in water at a ratio of 1/50 (*w*/w) in a centrifuge tube at room temperature. The solutions were then incubated in a water bath at different temperatures (40 °C, 60 °C, 80 °C, and 100 °C) for 30 min each. Subsequently, the samples were centrifuged at 5100 ×*g* for 10 min. The supernatant was collected in a pre-weighed evaporating dish (W_2, g) and dried to a constant weight at 105 ± 2 °C. The mass of the evaporating dish and residue (W_3, g) were then recorded. The WSI was determined using the Eq. (10) as provided below:

$$WSI\ (g/g) = (W_3 - W_2)/W_2 \times 100 \quad (10)$$

2.8. Surface microstructure of SSPL powder

The SSPL powder's morphology was examined using a scanning electron microscope (SEM) (SU8010, Hitachi Co., Ltd., Tokyo, Japan). The observation was conducted at an accelerating voltage of 10 kV. Before the examination, the dried SSPL powder was attached to a metal iron block using conductive glue, coated with gold, and then imaged at a 2000 × magnification.

2.9. Fourier transform infrared spectroscopy (FTIR)

The SSPL powder was coated with potassium bromide (KBr) and then compressed into pellets for analysis. A FTIR spectrometer (Nicolet 5700, Perkin Elmer Instrument Co., Ltd., Massachusetts, USA) was used to capture the FTIR spectra of the SSPL powder. The measurements were taken at a resolution of 4 cm^{-1} with 32 scans per sample covering the range of wavenumbers from 4000 to 400 cm^{-1} (Zhu et al., 2022).

2.10. X-ray diffraction spectroscopy (XRD)

An X-ray diffractometer (D8, Bruker AXS Co., Inc., Karlsruhe, Germany) was utilized to capture the XRD pattern of SSPL powder. The diffraction angle (2θ) range examined was from 5° to 50°, with step angle of 0.02° and a scan rate of 0.1 s. The crystallinity index was determined using the following Eq. (11):

$$CrI\ (\%) = ((I_{002} - I_{am})/I_{002})^*100 \quad (11)$$

where the intensities of the diffraction peaks at 2θ values near 22° and 18° are denoted by I_{002} and I_{am}, respectively.

2.11. Differential scanning calorimetry (DSC)

Approximately 20 mg of SSPL powder was carefully placed in a hermetically sealed aluminum pan and covered with a cap. Calorimetric analyses were conducted using a differential scanning calorimetry (DSC-60 A, Shimadzu Co., Ltd., Shanghai, China) by scanning from 20 to 120 °C at a heating rate of 10 °C/min in a dry nitrogen atmosphere.

2.12. Antioxidant activities of SSPL powder

2.12.1. Preparation of SSPL powder extracts

Firstly, 0.1 g of SSPL powder was weighed and diluted to 50 mL with distilled water. Meanwhile, the extraction took place in an ultrasonic bath (SB-5200DT, Scientz Biotechnology Co., lnc., Ningbo, China) at the operating power, frequency, and temperature of 400 W, 40 kHz and 40 °C, respectively for 30 min. Then the SSPL powder extracts were centrifuged at 4000 ×*g* for 15 min and the upper layer extract was frozen in a refrigerator at −20 °C for the antioxidant activities analyses.

2.12.2. DPPH radical scavenging assay

The scavenging activity of DPPH radical was evaluated following the procedure outlined by Liu et al. (2021). To summarize, 2 mL of SSPL powder extract was combined with 2 mL of DPPH reagent (0.004 % (*w/v*) in methanol). The mixture was agitated, kept in darkness for 30 min, and then the absorbance was recorded at 517 nm using a spectrophotometer (U3V-2550, Shimadzu Co. Ltd., Tokyo, Japan). Sodium selenite served as the inorganic Se control in this experiment, and vitamin C was used as the positive control. The percentage of DPPH radical scavenging activity was determined using the following Eq. (12) below:

$$\textit{DPPH radical scavenging capacity}\ (\%) = (A_0 - A_1)/A_0 \times 100 \quad (12)$$

Where A_0 represents the absorbance of the methanolic DPPH solution without any samples, while A_1 represents the absorbance of the samples being tested.

2.12.3. ABTS radical scavenging assay

The ABTS radical scavenging activity was assessed using the method outlined by Luo et al. (2021). An ABTS stock solution was prepared by mixing 7 mmol/L ABTS with 2.45 mmol/L potassium persulfate in equal volumes and allowing the reaction to take place in the dark for 14 h at 25 °C. The stock solution was then diluted with PBS (pH 7.0) until it reached an absorbance of 0.70 (± 0.2) at 734 nm. Next, 3 mL of the ABTS solution was combined with 1 mL of SSPL powder extracts and incubated at 25 °C for 6 min. The absorbance was then measured at 734 nm. Distilled water served as the blank control, vitamin C as the positive control, and sodium selenite as the inorganic Se control. The ABTS scavenging activity was determined using the Eq. (13) below:

$$\textit{ABTS radical scavenging activity}\ (\%) = (A_0 - A_1)/A_0 \times 100 \quad (13)$$

where A_0 represents the absorbance of the blank, while A_1 represents the absorbance of the samples.

2.12.4. Hydroxyl radical scavenging assay

The scavenging activity of hydroxyl radicals was evaluated following the method described by Gao et al. (2019). A mixture of 1 mL of 2 mg/mL samples (SSPL powder extracts, vitamin C, and sodium selenite) was combined evenly with 1 mL of salicylic acid-ethanol solution (9 mmol/L), 1 mL of ferrous sulfate solution (9 mmol/L), and 1 mL of aqueous hydrogen peroxide (8.8 mmol/L). The mixture was then placed in the dark at 37 °C for 20 min with constant shaking. The absorbance at 510 nm was recorded, with vitamin C serving as the positive control, distilled water as the blank control, and sodium selenite as the inorganic Se control. The hydroxyl radical scavenging activity was calculated using the Eq. (14) provided below:

$$\textit{Hydroxyl radical scavenging activity}\ (\%) = 1 - [(A_1 - A_2)/A_0] \times 100 \quad (14)$$

where A_0 represents the absorbance of the blank (no sample present), A_1 denotes the absorbance of the samples, and A_2 stands for the absorbance of the samples without the addition of H_2O_2 solution.

2.12.5. Superoxide radical scavenging assay

The scavenging activity of superoxide radicals was evaluated using the method by Gao et al. (2019). In this method, 1 mL of 2 mg/mL samples (SSPL powder extracts, vitamin C, or sodium selenite) were thoroughly mixed with 4.5 mL of 0.05 mol/L Tris-HCl buffer (pH 8.2) and then allowed to incubate at 25 °C for 20 min. Subsequently, 0.5 mL of 25 mmol/L pyrogallic acids was added to the solution at 30 °C for 5 min while shaking vigorously. Following this, 1 mL of 8 mol/L HCl was introduced to initiate the reaction, and the absorbance was then measured at 320 nm. Distilled water was utilized as the blank control, vitamin C served as the positive control in the experiment, and sodium selenite was employed as the inorganic Se control. The superoxide anion radical scavenging activity was determined using the Eq. (15) provided below:

$$\textit{Superoxide radical scavenging activity}\ (\%) = 1 - [(A_1 - A_2)/A_0] \times 100 \quad (15)$$

where A_0 represents the absorbance of the blank (no sample present), A_1 is the absorbance of the samples, and A_2 signifies the absorbance of the samples (without the addition of pyrogallic acid).

2.12.6. Reducing power assay

The reducing power was assessed using the method described by Li et al. (2020). In short, 1 mL of 2 mg/mL samples (SSPL powder extracts, Vc, and sodium selenite) were mixed with 3 mL of 0.2 mol/L sodium phosphate buffer (pH 6.6,) and 2.5 mL of 1 % potassium ferricyanide. The mixture was then incubated in a 50 °C water bath for 25 min and rapidly cooled to room temperature. Subsequently, 2.5 mL of 10 % trichloroacetic acid was introduced to the mixture, which was then centrifuged at 2100 ×*g* for 10 min at 4 °C. Next, 2.5 mL of the upper layer extract, 0.5 mL of 0.1 % ferric chloride and 2.5 mL of distilled water were mixed. Then, the optical density at 700 nm was measured after a 30-min incubation. Distilled water was used as the blank control, vitamin C served as the positive control, and sodium selenite was utilized as the inorganic Se control. An increase in absorbance indicated an increase in reducing power.

2.13. Sensory evaluation

2.13.1. E-nose

An electronic nose, specifically the PEN 3 model from Airsense Analytics Corp in Schwerin, Germany, was utilized to analyze the smell characteristics of SSPL powder. Each sensor in the e-nose displayed unique response characteristics, such as detecting aromatic compounds, nitrogen oxide, ammonia, hydrogen, alkenes, methane, sulfide compounds, alcohols, and various other organic compounds. The SSPL powder was enclosed in plastic wrap and subjected to analysis following the methodology outlined by Shao et al. (2023).

2.13.2. E- tongue

The taste profile of SSPL powder was examined using an electronic tongue (SA402B, Insent Company, Japan). The test sensors were labeled as CA0 (for sourness), CT0 (for saltiness), AAE (for umami), C00 (for bitterness), and AE1 (for astringency). Additionally, the reference sensors for aftertastes were identified as aftertaste-A (for astringency aftertaste) and aftertaste-B (for bitter aftertaste). SSPL powder was

Table 1
Effect of shear breaking and superfine grinding on color and chemical compositions of SSPL powder.

Samples	Color				Chemical compositions							
	L*	a*	b*	ΔE	Selenium (μg/g)	Total polyphenols (mg/g)	Total flavonoids (mg/g)	Crude protein (g/100 g)	Crude fiber (g/100 g)	Crude lipid (g/100 g)	Moisture (g/100 g)	Ash (g/100 g)
SB-Se0	52.36 ± 0.31^{c}	0.87 ± 0.10^{a}	22.42 ± 0.33^{c}	–	7.54 ± 1.39^{d}	139.82 ± 5.03^{d}	47.30 ± 0.78^{bc}	16.60 ± 0.68^{cd}	7.35 ± 0.53^{a}	0.04 ± 0.23^{c}	7.84 ± 0.46^{a}	7.54 ± 0.73^{a}
SB-Se0.5	53.51 ± 0.24^{b}	0.47 ± 0.04^{c}	21.95 ± 0.29^{d}	1.33 ± 0.18^{c}	24.39 ± 1.06^{c}	143.28 ± 3.77^{c}	47.22 ± 0.84^{c}	17.28 ± 0.36^{bc}	7.41 ± 0.44^{a}	0.04 ± 0.10^{c}	7.74 ± 0.27^{a}	8.34 ± 0.33^{a}
SB-Se1.0	52.25 ± 0.54^{c}	0.55 ± 0.06^{b}	22.97 ± 0.53^{c}	0.82 ± 0.50^{d}	36.09 ± 2.88^{b}	142.39 ± 7.49^{c}	46.70 ± 0.01^{c}	17.55 ± 0.31^{b}	7.07 ± 0.27^{a}	0.05 ± 0.22^{bc}	6.83 ± 0.37^{b}	7.67 ± 0.54^{a}
SB-Se2.0	50.43 ± 0.59^{d}	0.53 ± 0.08^{b}	22.71 ± 0.24^{c}	1.99 ± 0.57^{bc}	48.61 ± 1.24^{a}	143.62 ± 4.80^{c}	47.22 ± 0.84^{c}	19.33 ± 0.39^{a}	7.59 ± 0.58^{a}	0.05 ± 0.30^{bc}	6.47 ± 0.22^{b}	7.47 ± 0.40^{a}
SG-Se0	55.09 ± 0.67^{a}	0.32 ± 0.04^{d}	24.04 ± 0.10^{b}	3.24 ± 0.51^{a}	9.69 ± 0.74^{d}	146.30 ± 7.17^{b}	49.34 ± 0.99^{a}	16.35 ± 0.33^{d}	7.51 ± 0.29^{a}	0.08 ± 0.31^{a}	6.76 ± 0.32^{b}	8.50 ± 1.04^{a}
SG-Se0.5	53.19 ± 0.37^{b}	0.38 ± 0.04^{d}	25.33 ± 0.57^{a}	3.08 ± 0.52^{a}	25.44 ± 1.48^{c}	147.98 ± 7.21^{b}	48.76 ± 0.99^{a}	17.12 ± 0.77^{bcd}	7.25 ± 0.39^{a}	0.07 ± 0.14^{b}	6.78 ± 0.25^{b}	8.74 ± 0.95^{a}
SG-Se1.0	53.14 ± 0.72^{b}	0.32 ± 0.02^{d}	24.09 ± 0.62^{b}	2.09 ± 0.21^{b}	36.76 ± 1.38^{b}	145.52 ± 6.09^{bc}	48.05 ± 0.25^{abc}	17.26 ± 0.51^{bc}	7.68 ± 0.43^{a}	0.07 ± 0.27^{b}	6.49 ± 0.22^{b}	7.84 ± 0.39^{a}
SG-Se2.0	55.14 ± 0.26^{a}	0.31 ± 0.02^{d}	23.68 ± 0.47^{bc}	3.12 ± 0.27^{a}	50.40 ± 1.60^{a}	150.11 ± 5.40^{a}	48.69 ± 1.06^{ab}	19.11 ± 0.23^{a}	7.56 ± 0.29^{a}	0.06 ± 0.14^{b}	6.69 ± 0.40^{b}	8.15 ± 0.40^{a}

Different letters indicate significant differences between groups ($P < 0.05$).

Table 2
Particle size, flow, and hydration characteristics of SSPL powder.

Samples	Particle size (μm)	θ (°)	α (°)	ρ_b ($\times 10^3$ kg/m^3)	ρ_t ($\times 10^3$ kg/m^3)	WHC (g/g)	OHC (g/g)	FTS (g/g)	WSC (mL/g)	WSI (g/g)				CrI (%)
										40 °C	60 °C	80 °C	100 °C	
SB-Se0	72.66 ± 4.82^{a}	29.95 ± 0.99^{b}	34.06 ± 0.98^{b}	0.40 ± 0.01^{a}	0.61 ± 0.02^{ab}	6.13 ± 0.08^{ab}	1.99 ± 0.05^{bc}	0.78 ± 0.01^{a}	4.00 ± 0.28^{b}	0.21 ± 0.01^{b}	0.29 ± 0.01^{b}	0.26 ± 0.02^{b}	0.24 ± 0.01^{b}	11.15 ± 0.01^{a}
SB-Se0.5	74.75 ± 2.56^{a}	30.58 ± 0.55^{b}	36.34 ± 0.75^{b}	0.39 ± 0.01^{a}	0.63 ± 0.01^{a}	6.72 ± 0.18^{a}	2.28 ± 0.08^{b}	0.79 ± 0.01^{a}	4.10 ± 0.14^{b}	0.22 ± 0.01^{b}	0.30 ± 0.01^{b}	0.29 ± 0.01^{a}	0.25 ± 0.02^{b}	10.08 ± 0.01^{a}
SB-Se1.0	72.51 ± 3.49^{a}	29.18 ± 0.80^{b}	34.58 ± 0.25^{b}	0.38 ± 0.01^{a}	0.60 ± 0.02^{ab}	6.77 ± 0.19^{a}	2.62 ± 0.04^{a}	0.76 ± 0.01^{a}	4.30 ± 0.14^{b}	0.23 ± 0.01^{b}	0.31 ± 0.01^{b}	0.29 ± 0.01^{a}	0.25 ± 0.03^{b}	12.85 ± 0.01^{a}
SB-Se2.0	75.67 ± 6.28^{a}	28.74 ± 0.43^{b}	35.10 ± 0.99^{b}	0.40 ± 0.01^{a}	0.59 ± 0.01^{ab}	6.61 ± 0.17^{a}	2.11 ± 0.14^{bc}	0.80 ± 0.42^{a}	4.30 ± 0.14^{b}	0.22 ± 0.01^{b}	0.30 ± 0.01^{b}	0.28 ± 0.02^{b}	0.23 ± 0.04^{b}	12.37 ± 0.01^{a}
SG-Se0	26.50 ± 4.14^{b}	43.14 ± 0.36^{a}	48.37 ± 0.30^{a}	0.26 ± 0.01^{b}	0.54 ± 0.01^{b}	4.27 ± 0.25^{b}	1.74 ± 0.14^{d}	0.72 ± 0.01^{b}	7.60 ± 0.28^{a}	0.24 ± 0.02^{a}	0.34 ± 0.02^{a}	0.30 ± 0.02^{a}	0.26 ± 0.01^{a}	4.97 ± 0.01^{b}
SG-Se0.5	24.27 ± 4.59^{b}	49.80 ± 0.56^{a}	52.66 ± 0.67^{a}	0.30 ± 0.01^{b}	0.51 ± 0.01^{b}	4.47 ± 0.15^{b}	1.80 ± 0.14^{cd}	0.60 ± 0.01^{cd}	7.60 ± 0.28^{a}	0.24 ± 0.01^{a}	0.35 ± 0.02^{a}	0.31 ± 0.01^{a}	0.28 ± 0.03^{a}	5.37 ± 0.01^{b}
SG-Se1.0	23.50 ± 3.53^{b}	48.74 ± 0.70^{a}	51.72 ± 0.65^{a}	0.28 ± 0.01^{b}	0.52 ± 0.02^{b}	4.58 ± 0.16^{b}	1.81 ± 0.07^{cd}	0.58 ± 0.01^{d}	8.10 ± 0.14^{a}	0.27 ± 0.01^{a}	0.35 ± 0.01^{a}	0.31 ± 0.01^{a}	0.29 ± 0.01^{a}	4.98 ± 0.01^{b}
SG-Se2.0	24.37 ± 5.15^{b}	49.70 ± 0.42^{a}	53.61 ± 0.68^{a}	0.29 ± 0.01^{b}	0.54 ± 0.01^{b}	4.42 ± 0.14^{b}	1.77 ± 0.10^{d}	0.65 ± 0.01^{c}	8.10 ± 0.14^{a}	0.26 ± 0.01^{a}	0.34 ± 0.01^{a}	0.31 ± 0.01^{a}	0.27 ± 0.02^{a}	6.11 ± 0.01^{b}

Different letters indicate significant differences between groups ($P < 0.05$).

diluted in distilled water at a ratio of 1/1000 (*w/v*) and then centrifuged at 5100 ×*g* for 5 min. The analysis was carried out following the procedure outlined by Shen et al. (2023).

2.14. Statistical analysis

The results were presented as the mean ± standard deviation (SD) from a minimum of three independent experiments. Statistical analysis was performed using SPSS software 20.0 (SPSS Inc., USA) with analysis of variance (ANOVA). The cluster analysis and the Spearman correlation analysis were performed using RStudio software (Boston, MA, USA). Significant differences between means were assessed using Duncan's multiple-range test at a significance level of 5 %.

3. Results and discussion

3.1. Chemical compositions of SSPL powder

The Se contents of different parts of the sweet potato plant under the same Se application conditions were first determined. It was found that with the increase of Se concentration (foliar application), the Se contents in the leaves (7.54–48.61 g/100 g) (Table 1), stems (4.50–24.07 g/100 g) and petioles (2.31–26.53 g/100 g) were also increased. It showed that the exogenous Se sprayed on the leaf surface was successfully transferred to the interior of leaves, and the content of Se in sweet potato leaves was the highest. Therefore, the sweet potato leaves were used for the following experiments.

As shown in Table 1, marked differences in chemical composition were detected in superfine grinding samples. The total polyphenols,

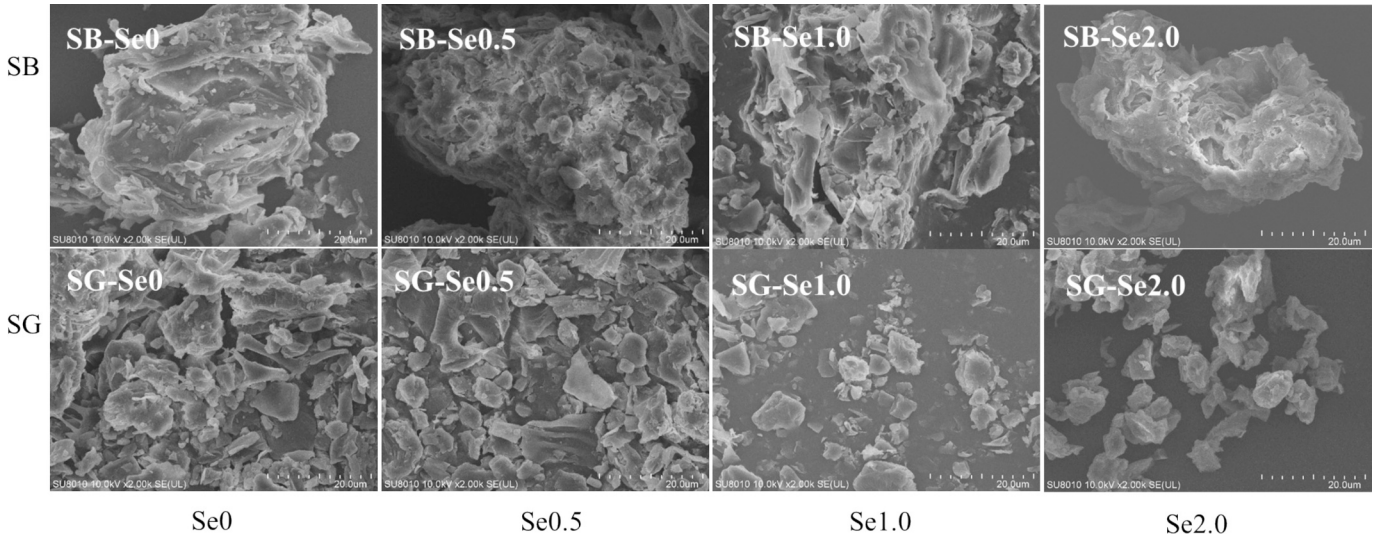

Fig. 1. SEM micrographs (× 2000) of SSPL powder with shear breaking and superfine grinding.

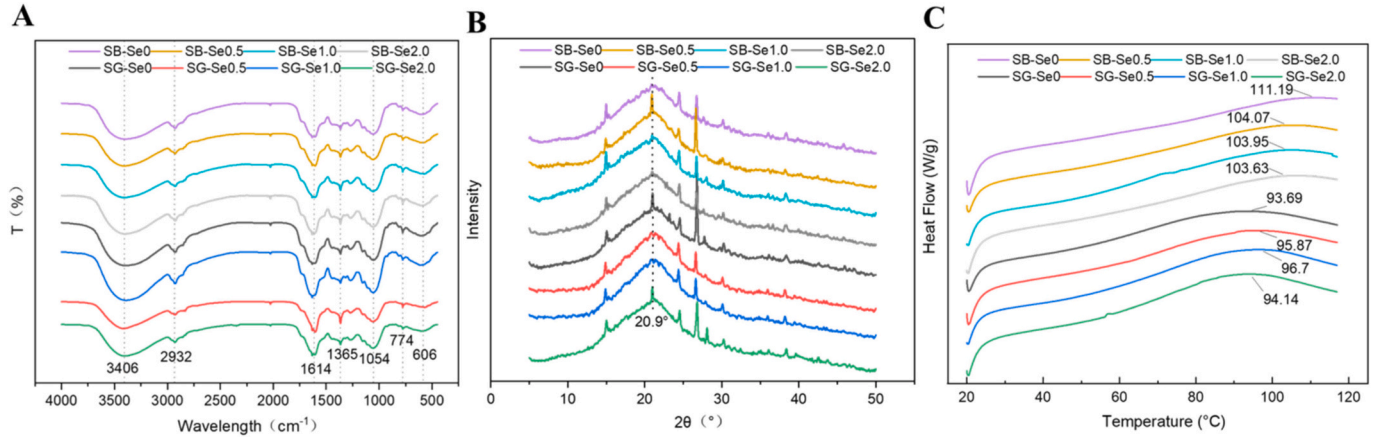

Fig. 2. FTIR (A), XRD (B), and DSC (C) curves of SSPL powder with shear breaking and superfine grinding.

flavonoids, and crude fat contents were increased following the process of superfine grinding. This was attributed to the cell wall rupture of the superfine grinding samples, which improved the solubilization and extraction of polyphenols, flavonoids, and crude fat (Kaur et al., 2023). Although the crude protein content was slightly lower after superfine grinding, the difference was not statistically significant ($P > 0.05$). This may be attributed to the fact that the degree of cellular structural damage increased as the particle size decreased, leading to protein transfer from intracellular to extracellular. In addition, the differences in the crude fiber, water, and ash contents of SSPL powder among different processing methods were not significant ($P > 0.05$).

By comparing the chemical composition of SSPL powder, it was found that the content of total Se and crude protein increased with the increase of foliar Se concentration (Table 1). The protein content of shear breaking SSPL powder increased from 16.60 g/100 g to 19.33 g/100 g, and the protein content of superfine grinding SSPL powder increased from 16.35 g/100 g to 19.11 g/100 g. When 2 mg/L Se was applied, the Se content of SSPL powder by shear breaking and superfine grinding were the highest at 48.61 μg/g and 50.40 μg/g, respectively. Se can cause an upregulation of the phenylpropanoid biosynthetic pathway, and the metabolites belong to the class of polyphenols and flavonoids, which play a central role in determining antioxidant activities (Mimmo et al., 2017). However, the total phenol and total flavonoids did not increase significantly with the increase of Se treatment concentration at the same crushing method ($P < 0.05$). Plants have complex internal regulatory and buffering mechanisms. SSPL may have its own homeostatic system that can resist the influence of external Se to a certain extent. When the Se concentration changes within a certain range, the plant can adjust its metabolism to maintain the relative stability of the content of important substances such as flavonoids and polyphenols (Dreyer et al., 2024). Se may interact with other elements or substances in the SSPL. These interactions may affect the uptake, transport, or utilization of nutrients related to polyphenol synthesis, thereby indirectly affecting the content of total polyphenols. Compared to shear breaking, SSPL after superfine grinding increased significantly the concentration of total phenols and total flavonoids ($P < 0.05$).

3.2. Mean particle size of SSPL powder

As shown in Table 2, the particle size range of shear breaking SSPL powder was 72.51–75.67 μm, while the superfine grinding SSPL powder were 23.5–27.84 μm. This demonstrated that compared with the shear breaking SSPL powder, the particle size of superfine grinding SSPL powder was smaller, which may result in improved bioavailability and solubility (Jiang et al., 2017). The two crushing methods could be used to produce SSPL powder with different particle sizes according to needs. Furthermore, there were no significant changes in the average particle size of SSPL powder at different Se levels.

Table 3
The DPPH, ABTS, superoxide radical, hydroxyl radical scavenging activity and reducing power of SSPL powder.

Samples	Antioxidant activities (%)				
	DPPH•	$ABTS^{+}$•	O_2^-•	•OH	Reducing power
SB-Se0	59.84 ± 0.67^{d}	82.94 ± 1.60^{cd}	27.02 ± 0.68^{d}	29.60 ± 0.53^{e}	0.53 ± 0.02^{f}
SB-Se0.5	62.37 ± 0.78^{cd}	83.78 ± 1.51^{c}	26.18 ± 0.23^{de}	30.81 ± 0.31^{de}	0.57 ± 0.02^{e}
SB-Se1.0	62.53 ± 0.63^{cd}	83.53 ± 1.00^{c}	28.22 ± 0.89^{d}	30.56 ± 0.75^{de}	0.57 ± 0.01^{e}
SB-Se2.0	63.18 ± 0.62^{c}	83.32 ± 0.94^{c}	28.18 ± 0.41^{d}	29.26 ± 0.64^{e}	0.62 ± 0.02^{d}
SG-Se0	64.26 ± 0.72^{bc}	84.74 ± 0.23^{b}	34.41 ± 0.91^{b}	31.24 ± 0.22^{d}	0.65 ± 0.01^{cd}
SG-Se0.5	65.01 ± 0.71^{b}	84.01 ± 1.19^{bc}	34.39 ± 0.11^{b}	31.55 ± 0.80^{d}	0.65 ± 0.02^{cd}
SG-Se1.0	64.20 ± 0.58^{bc}	85.91 ± 0.81^{b}	30.44 ± 0.68^{c}	34.30 ± 0.69^{c}	0.66 ± 0.03^{c}
SG-Se2.0	65.38 ± 0.68^{b}	84.43 ± 1.10^{b}	33.25 ± 0.46^{b}	31.34 ± 0.91^{d}	0.70 ± 0.01^{b}
Vc	96.29 ± 0.30^{a}	90.20 ± 0.72^{a}	92.72 ± 0.43^{a}	99.63 ± 0.13^{a}	4.32 ± 0.01^{a}
Sodium selenite	13.07 ± 0.50^{e}	24.03 ± 1.91^{d}	16.04 ± 0.14^{e}	62.29 ± 0.64^{b}	0.09 ± 0.06^{g}

Different letters indicate significant differences between groups ($P < 0.05$).

3.3. Color parameters of SSPL powder

The color values of different SSPL powder samples are shown in Table 1. By comparing the two crushing methods, as expected, the L*, b*, and ΔE* values of the superfine grinding SSPL powder increased significantly, while the a* value decreased compared with the shear breaking SSPL powder ($P < 0.05$). The brightness and yellowness increased after the superfine grinding treatment, attributed to the increased surface area and exposure of the internal structure resulting from the grinding process (Ahmed et al., 2019). Meanwhile, the increase in greenness of SSPL powder was associated with increased exposure to internal colored substances such as chlorophyll during superfine grinding (He et al., 2019).

By comparing four different foliar application Se concentrations, it was found that Se had a slight effect on the a* value with no significant difference detected between the L* and b* values. After Se enrichment, the a* value was reduced and the powder turned green, which could be attributed to Se affecting chlorophyll metabolism. Se significantly enhanced the levels of chlorophyll *a*, b, and total chlorophyll in garlic (Astaneh et al., 2019). Foliar application of Se nanoparticles at 2 μmol/L greatly can increase the chlorophyll content of pomegranate (Zahedi et al., 2019). The SSPL powder with brighter and more vivid colors is favorable in the food industry or as a food additive.

3.4. Flow properties of SSPL powder

Table 2 illustrated the angles of repose and slide values of different SSPL powder samples. The physical properties of the powder were not only related to the raw material but also to the crushing method. As a result, the angles of repose and slide values increased dramatically ($P < 0.05$) after superfine grinding SSPL powder has stronger rough adhesion and poorer fluidity than shear breaking SSPL powder. The findings are in line with the investigation on *Lycium ruthenicum* Murray powders (Zhang et al., 2020). The surface cohesion force of SSPL powder was increased with the decline of particle size due to van der Waals force and hydrogen bonding interactions, and the particles of SSPL powder were more prone to adsorb and agglomerate with each other, resulting in poor fluidity.

Bulk density is a key indicator of the fillability of SSPL powder during processing. It plays a crucial role in determining whether the final product can be packed into a specific container and also has a significant impact on the powder's handling and storage. In the context of the specific requirement for reducing weight, bulk density becomes even more relevant. The larger the bulk density, the better the filling of SSPL powder. As shown in Table 2, the bulk density and tap density of superfine grinding SSPL powder decreased significantly ($P < 0.05$) compared with shear breaking SSPL powder, which was consistent with the results of *Tremella aurantialba* powder (Zhao et al., 2018). The superfine grinding SSPL powder resulted in decreased filling capacity due to increased intracrystal voids and expanded interfacial area. After superfine grinding, the filling capacity of the superfine grinding SSPL powder significantly deteriorates as the result of the higher number of intracrystal voids and the increased interfacial area (Hu et al., 2012; Zhao et al., 2010). There were no significant differences in tilt angle, slip angle, bulk density, and tapping density between the 4 Se concentrations of SSPL powder.

3.5. Hydration properties of SSPL powder

WHC is a crucial property of powder, reflecting their ability to retain

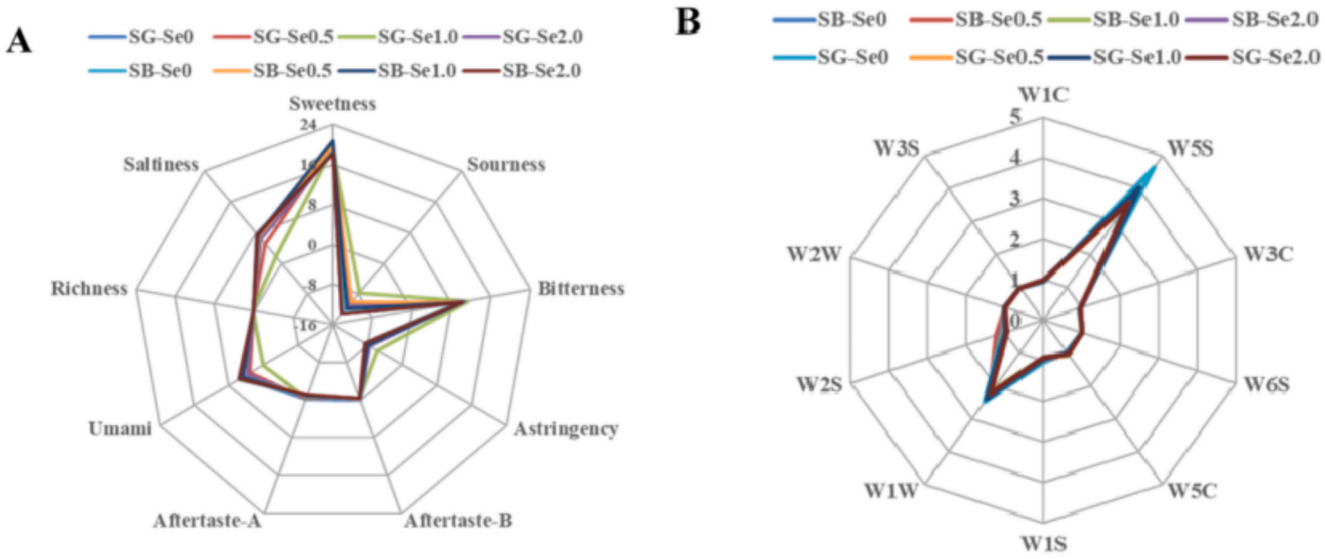

Fig. 3. Electronic tongue (A) and electronic nose (B) of SSPL powder with shear breaking and superfine grinding.

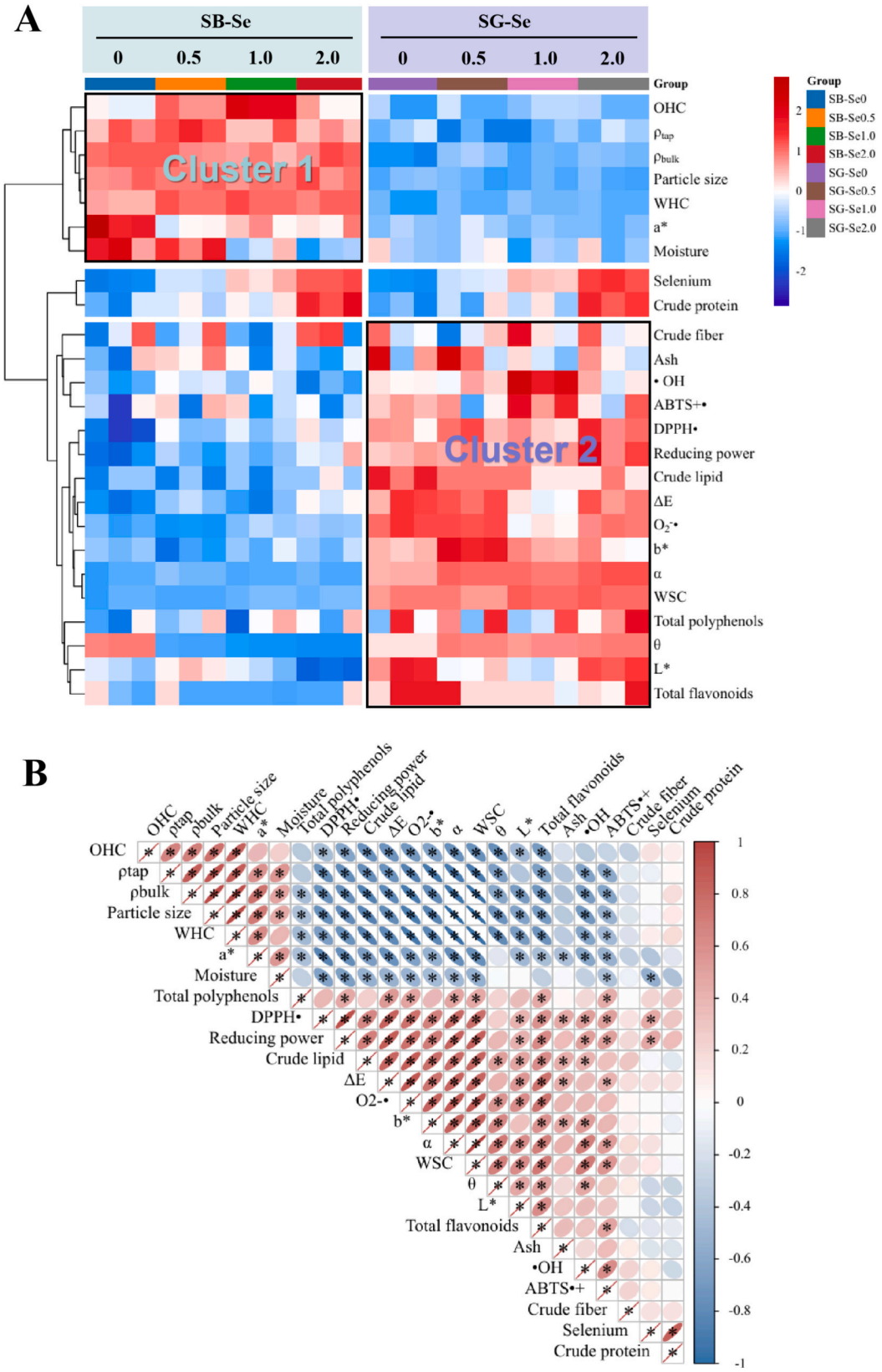

Fig. 4. The cluster heatmap (A) and correlation heatmap (B) of the indicators of the SSPL powder with shear breaking and superfine grinding. The * indicates significant differences between groups ($P < 0.05$).

water. As shown in Table 2, the WHC values of superfine grinding SSPL powder were significantly lower ($P < 0.05$) compared to shear breaking SSPL powder, which was consistent with the findings of *Flammulina velutipe* polysaccharide powder (Zhang et al., 2013) and *Moringa Oleifera* leaf powder (Huang et al., 2020). During superfine grinding, the polar amino acid residues exposed on the surface of the protein were destroyed. Meanwhile, the fibers that are prone to water swelling were interrupted (Huang et al., 2020), so that the hydration property was decreased.

OHC is an index to evaluate the ability of samples to absorb oil. According to Table 2, it was found that the OHC values of the superfine grinding SSPL powder were significantly reduced ($P < 0.05$) compared to the shear breaking SSPL powder, which was consistent with the findings of soybean residue powder (Li et al., 2020) and water dropwort powder (He et al., 2019). This may be due to the disruption of the porous structure of dietary fibers during ultrafine grinding and the exposure of hydrophilic groups.

FTS is expressed by water separation rate, and a low water separation rate indicates better FTS. As shown in Table 2, the water separation rate of SSPL powder was significantly decreased ($P < 0.05$) after superfine grinding, suggesting that superfine grinding could enhance the FTS of SSPL powder. The explanation may stem from the refined particle size of superfine grinding SSPL powder, which provides a larger particle surface area and consequently enhances the exposure of its hydrophilic groups. So that the superfine grinding SSPL powder, could reduce water loss during the thawing process, and improve the FTS of the SSPL powder.

WSC can reflect the water-binding capacity of SSPL powder. The larger the swelling value, the better the stability and suspension of the powder when dissolved in water. As shown in Table 1, the WSC of SSPL powder ranges of shear breaking and superfine grinding were 4–4.3 mL/g and 7–8.1 mL/g, respectively. Compared with shear breaking SSPL powder, the WSC values of the superfine grinding SSPL powder increased significantly ($P < 0.05$). A similar result was obtained in the characterization of soybean residue powder (Li et al., 2020). Superfine grinding can reduce the particle size of SSPL powder to a very small level, resulting in a significantly larger specific surface area. A larger specific surface area means that there are more surface sites available to interact with water molecules, facilitating water absorption and thus increasing the WSC. In contrast, shear breaking may not reduce the particle size as effectively, leading to a relatively small specific surface area and limited contact area with water, resulting in a lower WSC. Superfine grinding reduced the particle size of the powder, increasing its contact area with water. Furthermore, superfine grinding is likely to change the internal pore structure of the SSPL powder, making the pores more uniform and increasing the porosity. This porous structure can accommodate more water molecules, enhancing the water absorption capacity and swelling degree. Shear breaking may have less impact on the pore structure, and the original pore structure may not be conducive to efficient water absorption, resulting in a lower WSC. Therefore, each unit volume of powder can absorb more water, and the expansion force became higher (Zhao et al., 2010).

WSI is a key indicator of the hydration capacity of SSPL powder. Table 2 illustrated that the ideal temperature for WSI was 60 °C. superfine grinding SSPL powder showed higher WSI values compared to shear breaking SSPL powder at various temperatures, possibly because of the increased exposure of its hydrophilic groups through superfine grinding. The study indicated that superfine grinding SSPL powder demonstrated superior solubility and dispersibility, making it suitable for manufacturing tablets or capsules (Hu et al., 2012). Furthermore, SSPL powder with higher WHC and SC values had great potential as functional ingredients to prevent syneresis, modify texture and mouthfeel characteristics, as well as improve the reconstituability in the mix drinks (Wang et al., 2013). No noticeable discrepancies were detected in the hydration properties of SSPL powder with different levels of Se concentrations.

3.6. SEM analysis of SSPL powder

As shown in Fig. 1, the surface morphology after superfine grinding had changed greatly compared with shear breaking. The particles of superfine grinding SSPL powder were relatively smooth, fine, and uniform. It suggested that treatment with superfine grinding altered the physical characteristics of SSPL powder, particularly its shape and surface characteristics, which could potentially impact its physicochemical properties.

3.7. FTIR analysis of SSPL powder

Fig. 2A displayed the FTIR data of the SSPL powder samples with various grinding treatments and Se concentrations. A noticeable broad absorption peak at 3406 cm^{-1} was attributed to O—H and C—O bonds within phenol and cellulose, suggesting the presence of carbohydrates in the sample (Zhang et al., 2013). The band at 2932 cm^{-1} was indicative of the oscillation of C—H bonds in cellulose and proteins (Zhao et al., 2015). The absorption peak at 1614 cm^{-1} was indicative of the stretching motion of C—H bonds found in aromatic compounds, carboxylic acids, and polyphenols (Xiong et al., 2021). The band at 1054 cm^{-1} illustrated that SSPL powder contained pyranose monomers (Zhang et al., 2013). The characteristic peak at 776 cm^{-1} indicated the vibration of Se═O (Li et al., 2017), and the absorption peak at 606 cm^{-1} was characteristic of the symmetric stretching vibration of Se-O-C (Gao et al., 2021; Xiang et al., 2022). Furthermore, Fig. 2A showed that the principal absorption peaks in the FTIR spectra of SSPL powder remained consistent, indicating that no new chemical groups were formed after grinding. However, there were variations in the intensities of the peaks among the SSPL powder samples. The superfine grinding SSPL powder exhibited the highest absorbance levels across all peaks, including those associated with phenolic compounds and polysaccharides such as 3406, 2932, and 1054 cm^{-1} (Fig. 2A), thus contributing to enhanced antioxidant properties. The results indicated that the major functional groups of the SSPL powder remained unchanged and was successfully enriched with Se after superfine grinding.

3.8. XRD analysis of SSPL powder

As shown in Fig. 2B, the XRD patterns of the samples were similar. The position and width of crystallization peaks among these samples were not significantly different. They were prominent 2θ peaks around 15° and 22°, which were attributed to cellulose crystals (Huang et al., 2018). However, the crystallinities exhibited slight differences (Table 2), indicating that superfine grinding resulted in the destruction of the crystalline regions in SSPL powder, leading to a decrease in crystallinity. It has been reported that the mechanical stress induced by superfine grinding disrupts the intramolecular hydrogen bonds in SSPL powder, causing the degradation of hemicellulose and cellulose and the generation of soluble sugars and new amorphous cellulose. These changes altered the balance between amorphous and crystalline domains in SSPL powder (Zhao et al., 2015). The result was consistent with the results of FTIR (Fig. 2A). Regarding Se concentration, the XRD patterns among these samples were not significantly different.

3.9. Thermal property analysis of SSPL powder

As shown in Fig. 2C, the SSPL powder underwent phase transition during the heating process, which was an endothermic process, and the peak temperature was between 93.69 °C and 111.19 °C. Apparently, the peak temperature after superfine grinding was lower than that of shear breaking, indicating that shear breaking SSPL powder had higher thermal stability. Particle size affects peak temperature, which may be due to the high intensity collision of the sample with the agate beads during the superfine grinding process, exposing the polysaccharides and proteins, thus lowering the peak temperature (Huang et al., 2020).

Furthermore, the peak temperature of SG-Se0 was the lowest at 93.69 °C. It was found that following the increase of Se concentration, the peak temperature of the SSPL powder also increased, leading to improved thermal stability of the powder.

3.10. Antioxidant activities analysis of SSPL powder

In this study, the antioxidant activities of SSPL powder were evaluated using DPPH, ABTS, hydroxyl, and superoxide radical scavenging activities, as well as reducing power (Table 3). Comparing the two crushing methods, it was found that the SSPL powder obtained by superfine grinding exhibited the highest scavenging activities against DPPH•, $ABTS^{+}$•, O_2^{-}•, and •OH. Sweet potato leaves are a significant source of polyphenol compounds (Nguyen et al., 2021). Previous studies indicated that the antioxidant activities of sweet potato leaves may be attributed to the presence of epicatechin, catechin, rutin, and chlorogenic acid (Suliman et al., 2021). Furthermore, as the degree of grinding increased, the particle size of the SSPL powder decreased, leading to the destruction of its particle structure and subsequently enhancing the release of antioxidant substances. It was found that antioxidant substances, such as flavonoids and polyphenols, could significantly improve the scavenging activity against free radicals. Furthermore, the reducing power of superfine grinding SSPL powder was increased.

Based on the findings above, it can be concluded that among the five evaluation methods used, the antioxidant activities of superfine grinding SSPL powder were significantly higher than those of shear breaking SSPL powder ($P < 0.05$). This indicated that the crushing method could affect the antioxidant activities of the samples significantly. The grinding process resulted in a reduction in particle size and disruption of the sample structure, leading to the release of more antioxidants such as flavonoids and polyphenols. As a result, the antioxidant activities of the samples were enhanced.

Therefore, superfine grinding of SSPL powder offers two main benefits. Firstly, it reduces particle size, increasing the specific surface area. This exposes more active sites of antioxidant components like flavonoids and polyphenols, enabling more extensive contact with free radicals in the test system, thus improving free-radical scavenging efficiency and enhancing antioxidant activity. Secondly, it modifies the surface properties of powder particles, such as surface charge and hydrophilicity. Changes in surface properties can affect the powder-environment interaction.

3.11. Flavor evaluation of SSPL powder

Sweet potato leaves are rich in nutrients such as fiber, amino acids, and trace elements. Previous studies showed that the nutrients in sweet potato leaves can be affected by different crushing methods and Se enrichment concentrations (Wang et al., 2022; Zhang et al., 2021). Foliar Se enrichment increased Se concentration in sweet potato leaves. Thus, SSPL powder has the potential to be used as a novel solid beverage.

It can be seen from Fig. 3A that each taste sensor responded to SSPL powder but with different sensitivities. The sweetness, sourness, bitterness, and astringency of SSPL powder had higher response intensity than the umami and salty. It indicated that the SSPL powder tasted sweet and sour first, followed by bitterness and astringency, and had slightly aftertaste-astringent. It's worth noting that no significant disparity ($P > 0.05$) existed among SSPL powder with varying treatments. These results reflected that the taste value of SSPL powder with different crushing methods and different Se-enriched concentrations remained unchanged.

Aroma characteristics are associated with changes in nutritional content and diet quality, thereby may ultimately determine consumer approval or rejection of the product. As shown in Fig. 3B, the content of nitrogen oxides, organic sulfides, and terpenoids was higher, which could be closely related to the unique fragrance of SSPL powder. At the same time, the response trends of volatile flavor compounds of SSPL powder with different crushing methods and different Se concentrations were the same.

3.12. Correlation analysis of the indicators of the SSPL powder with shear breaking and superfine grinding

As shown in Fig. 4A, the heatmap was clustered in three clusters, especially cluster 1 and cluster 2. In cluster 1, the indicators (OHC, ρ_{tap}, ρ_{bulk}, particle size, WHC, a*, and moisture) present positive correlation to shear breaking SSPL powder. In cluster 2, the indicators (crude fiber, ash, •OH and DPPH• scavenging activities, reducing power, crude lipid, ΔE, O_2^{-}•, b*, α, WSC, total polyphenol, θ, L*, total flavonoids, and moisture) present positive correlation to superfine grinding SSPL powder. Thus, superfine grinding could improve crude fiber, crude lipid, total flavonoids, total polyphenol, and enhance the antioxidant activity compared to shear breaking. Superfine grinding could promote the WSC of the SSPL powder, while shear breaking reduced the OHC and WHC. However, superfine grinding promoted the color of SSPL powder to turn yellow. The two treatments have no significant effect on the Se content of SSPL powder. As shown in the correlation heatmap (Fig. 4B), Se content showed a significant ($P < 0.05$) positive correlation to crude protein, DPPH• scavenging activity, and reducing power, especially crude protein. Se is more efficiently transformed from inorganic to organic form in the ecological chain. The organic form of Se is primarily created during the metabolism of certain organic small molecules, such as amino acids in the form of R-Se-R, and macromolecular products, such as Se-enriched peptides, Se-enriched protein, and Se-enriched polysaccharides (Chen et al., 2021). Thus, Se enrichment can enhance the content of the crude protein and the antioxidant activities (DPPH• scavenging activity and reducing power).

4. Conclusions

In summary, this study found that Se enrichment can improve the content of crude protein, DPPH• scavenging activities, and reducing power of the samples. Superfine grinding can significantly improve the properties of SSPL powder. This includes brighter color, smaller particle size, improved hydration properties, and enhanced antioxidant activities compared to shear breaking. Se enrichment can enhance the content of the crude protein, DPPH• scavenging activity, and reducing power. The findings also suggested that these techniques cannot impact the flavor of SSPL powder, making it a promising option for use in food industry, particularly as a new solid beverage candidate. Additionally, this study confirmed successful Se enrichment in SSPL powder without affecting its major functional groups, further highlighting the potential for comprehensive utilization of SSPL powder.

CRediT authorship contribution statement

Qi Gao: Writing – original draft, Methodology. **Jia-Nan Chen:** Writing – original draft, Software, Data curation, Conceptualization. **Yu-Lu Tian:** Investigation, Formal analysis. **Miao-Miao Hao:** Data curation. **Xuan-Li Sha:** Software, Investigation. **Ang Li:** Formal analysis. **Xue Peng:** Data curation. **Tao Yu:** Writing – review & editing. **Xue-Jun Gu:** Writing – review & editing. **You-Lin Xue:** Writing – review & editing, Project administration, Funding acquisition.

Declaration of competing interest

The authors declare that they have no known competing financial interests or personal relationships that could have appeared to influence the work reported in this paper.

Acknowledgments

This work was supported by the National Natural Science Foundation

of China (31201285), the China Postdoctoral Science Foundation (2017M611752), the Liaoning Revitalization Talents Program (XLYC1807270), the Serving Local Project of the Education Department of Liaoning Province, China (LJKFZ20220183), the Taizhou Innovative Talents Program (202149), the Basic Research Project of Liaoning University (LJKZD202404), and the Youth Research Foundation Project of Liaoning University (LDZDJC2403).

Appendix A. Supplementary data

Supplementary data to this article can be found online at https://doi.org/10.1016/j.fochx.2025.102266.

Data availability

No data was used for the research described in the article.

References

Ahmed, J., Thomas, L., & Arfat, Y. A. (2019). Functional, rheological, microstructural and antioxidant properties of quinoa flour in dispersions as influenced by particle size. *Food Research International, 116*, 302–311. https://doi.org/10.1016/j.foodres.2018.08.039

Astaneh, R. K., Bolandnazar, S., Nahandi, F. Z., & Oustan, S. (2019). Effects of selenium on enzymatic changes and productivity of garlic under salinity stress. *South African Journal of Botany, 121*, 447–455. https://doi.org/10.1016/j.sajb.2018.10.037

Chen, N., Zhao, C. H., & Zhang, T. H. (2021). Selenium transformation and selenium-rich foods. *Food Bioscience, 40*, Article 100875. https://doi.org/10.1016/j.fbio.2020.100875

Dhiman, A., & Prabhakar, P. K. (2021). Micronization in food processing: A comprehensive review of mechanistic approach, physicochemical, functional properties and self-stability of micronized food materials. *Journal of Food Engineering, 292*, Article 110248. https://doi.org/10.1016/j.jfoodeng.2020.110248

Dobrzyńska, M., Drzymała-Czyż, S., Woźniak, D., Drzymała, S., & Przysławski, J. (2023). Natural sources of selenium as functional food products for chemoprevention. *Foods, 12*, 1247. https://doi.org/10.3390/foods12061247

Dong, Z., Xiao, Y. Q., & Wu, H. (2021). Selenium accumulation, speciation, and its effect on nutritive value of *Flammulina velutipes* (Golden needle mushroom). *Food Chemistry, 15*, Article 128667. https://doi.org/10.1016/j.foodchem.2020.128667

Dreyer, I., Hernández-Rojas, N., Bolua-Hernández, Y., de los Angeles Tapia-Castillo, V., Astola-Mariscal, S. Z., Díaz-Pico, E., … Michard, E. (2024). Homeostats: The hidden rulers of ion homeostasis in plants. *Quantitative Plant Biology, 5*, Article e8. https://doi.org/10.1017/qpb.2024.8

FAO. (2021). *Statistics Division of Food and Agriculture Organization of the United Nations*. http://www.fao.org/faostat/zh/#data/QC.

Gao, Q., Liu, Z. H., Wu, J. L., Geng, Y., Zhang, Q., Tie, M., … Xue, Y. L. (2019). Foliar application is an effective method for incorporating selenium into peanut leaf proteins with antioxidant activities. *Food Research International, 126*, Article 108617. https://doi.org/10.1016/j.foodres.2019.108617

Gao, Q., Wu, J. L., Jiang, L. P., Sun, S. Q., Gu, X. J., Tie, M., … Xue, Y. L. (2021). Se-O bond is unique to high se enriched sweet potato stem protein with better antioxidant ability. *Foods, 10*, 3064. https://doi.org/10.3390/foods10123064

He, S., Tang, M., Sun, H., Ye, Y., Cao, X., & Wang, J. (2019). Potential of water dropwort (*Oenanthe javanica* DC.) powder as an ingredient in beverage: Functional, thermal, dissolution and dispersion properties after superfine grinding. *Powder Technology, 353*, 516–525. https://doi.org/10.1016/j.powtec.2019.05.048

Hernández-Grijalva, M. I., Serrano-Sandoval, S. N., Gutiérrez-Uribe, J. A., Serna-Saldivar, S. O., Milán-Carrillo, J., Antunes-Ricardo, M., … Guardado-Félix, D. (2022). Application of protein fractions from selenized sprouted chickpeas as emulsifying agents and evaluation of their antioxidant properties. *Food and Bioproducts Processing, 136*, 59–66. https://doi.org/10.1016/j.fbp.2022.09.010

Hong, W., Duan, M., Wang, Y., Chen, Y., Mo, Z., Qi, J., … Tang, X. (2024). Enriching iodine and regulating grain aroma, appearance quality, and yield in aromatic rice by foliar application of sodium iodide. *Rice Science, 31*, 328–342. https://doi.org/10.1016/j.rsci.2024.02.005

Hu, J., Chen, Y., & Ni, D. (2012). Effect of superfine grinding on quality and antioxidant property of fine green tea powders. *LWT-Food Science Technology, 45*, 8–12.

Huang, J. Y., Liao, J. S., Qi, J. R., Jiang, W. X., & Yang, X. Q. (2021). Structural and physicochemical properties of pectin-rich dietary fiber prepared from citrus peel. *Food Hydrocolloids, 110*, Article 106140. https://doi.org/10.1016/j.foodhyd.2020.106140

Huang, X., Dou, J. Y., Li, D., & Wang, L. J. (2018). Effects of superfine grinding on properties of sugar beet pulp powders. *LWT-Food Science and Technology, 87*, 203–209. https://doi.org/10.1016/j.lwt.2017.08.067

Huang, X., Liang, K. H., Liu, Q., Qiu, J., Wang, J., & Zhu, H. (2020). Superfine grinding affects physicochemical, thermal and structural properties of *Moringa Oleifera* leaf powders. *Industrial Crops and Products, 151*, Article 112472. https://doi.org/10.1016/j.indcrop.2020.112472

Jia, Y., Nima, C., Yang, L., Wang, L., Wei, B., Li, Y., Li, H., Deji, Y., Zhao, S., Guo, M., Gong, H., Kong, C., Gu, L., Gesang, Z., & Li, R. (2023). Selenium and zinc intakes of staple grains and their correlation with urine selenium and zinc in the Tibetan rural residents along the Yarlung Zangbo River. *Nutrients, 15*, 2010. https://doi.org/10.3390/nu15082010

Jiang, L., Xu, Q. X., Qiao, M., Ma, F. F., Thakur, K., & Wei, Z. J. (2017). Effect of superfine grinding on properties of *Vaccinium bracteatum Thunb* leaves powder. *Food Science and Biotechnology, 26*, 1571–1578. https://doi.org/10.1007/s10068-017-0126-y

Kaur, G. J., Orsat, V., & Singh, A. (2023). An overview of different homogenizers, their working mechanisms and impact on processing of fruits and vegetables. *Critical Reviews in Food Science and Nutrition, 63*, 2004–2017. https://doi.org/10.1080/10408398.2021.1969890

Kavcic, A., Budic, B., & Vogel-Mikus, K. (2020). The effects of selenium biofortification on mercury bioavailability and toxicity in the lettuce-slug food chain. *Food and Chemical Tpxicology, 135*, Article 110939. https://doi.org/10.1016/j.fct.2019.110939

Kieliszek, M., & Sandoval, S. N. S. (2023). The importance of selenium in food enrichment processes. A comprehensive review. *Journal of Trace Elements in Medicine and Biology, 79*, Article 127260. https://doi.org/10.1016/j.jtemb.2023.127260

Li, G., Guo, W., Gao, X., Wang, Y., & Sun, S. (2020). Effect of superfine grinding on physicochemical and antioxidant properties of soybean residue powder. *Food Science and Nutrition, 8*, 1208–1214. https://doi.org/10.1002/fsn3.1409

Li, Q., Wang, W., Zhu, Y., Chen, Y., Zhang, W. J., Yu, P., … Wu, X. (2017). Structural elucidation and antioxidant activity a novel se-polysaccharide from se-enriched *Grifola frondosa*. *Carbohydrate Polymers, 161*, 42–52. https://doi.org/10.1016/j.carbpol.2016.12.041

Liu, Q., Cheng, J., Sun, X., & Guo, M. (2021). Preparation, characterization, and antioxidant activity of zein nanoparticles stabilized by whey protein nanofibrils. *International Journal of Biological Macromolecules, 167*, 862–870. https://doi.org/10.1016/j.ijbiomac.2020.11.043

Luo, D., Mu, T., & Sun, H. (2021). Profiling of phenolic acids and flavonoids in sweet potato (*Ipomoea batatas* L.) leaves and evaluation of their anti-oxidant and hypoglycemic activities. *Food. Bioscience, 39*, Article 100801. https://doi.org/10.1016/j.fbio.2020.100801

Mimmo, T., Tiziani, R., Valentinuzzi, F., Lucini, L., Nicoletto, C., Sambo, P., Scampicchio, M., Pii, Y., & Cesco, S. (2017). Selenium biofortification in *Fragaria* × *ananassa*: Implications on strawberry fruits quality, content of bioactive health beneficial compounds and metabolomic profile. *Frontiers in Plant Science, 8*, 1887. https://doi.org/10.3389/fpls.2017.01887

Nguyen, H. C., Chen, C. C., Lin, K. H., Chao, P. Y., & Huang, M. Y. (2021). Bioactive compounds, antioxidants, and health benefits of sweet potato leaves. *Molecules, 26*, 1820. https://doi.org/10.3390/molecules26071820

Shao, Y., Liu, X., Zhang, Z., Wang, P., Li, K., & Li, C. (2023). Comparison and discrimination of the terpenoids in 48 species of huajiao according to variety and geographical origin by E-nose coupled with HS-SPME-GC-MS. *Food Research International, 167*, Article 112629. https://doi.org/10.1016/j.foodres.2023.112629

Suliman, S., Yagi, S., Elbashir, A. A., Mohammed, I., Hussein, A., Ak, G., … Ferrante, C. (2021). Phenolic profile, enzyme inhibition and antioxidant activities and bioinformatics analysis of leaf and stem bark of *Ficus sycomorus* L. *Process Biochemistry, 101*, 169–178. https://doi.org/10.1016/j.procbio.2020.11.011

Tang, C. C., Ameen, A., Fang, B. P., Liao, M. H., Chen, J. Y., Huang, L. F., & Wang, Z. Y. (2021). Nutritional composition and health benefits of leaf-vegetable sweet potato in South China. *Journal of Food Composition and Analysis, 96*, Article 103714. https://doi.org/10.1016/j.jfca.2020.103714

Wang, H., Yang, S., Chen, Y., Wang, Z., Yuan, Y., & Yue, T. (2024). Comprehensive distribution and species of selenium in se-enriched *Pichia kudriavzevii* 1845. *Food Chemistry, 438*, Article 137966. https://doi.org/10.1016/j.foodchem.2023.137966

Wang, K., Fang, Q., He, P., Tu, Y., Liu, Z., & Li, B. (2024). Unveiling the potential of selenium-enriched tea: Compositional profiles, physiological activities, and health benefits. *Trends in Food Science & Technology, 145*, Article 104356. https://doi.org/10.1016/j.tifs.2024.104356

Wang, M., Leng, C., Zhu, Y., Wang, P., Gu, Z., & Yang, R. (2022). UV-B treatment enhances phenolic acids accumulation and antioxidant capacity of barley seedlings. *LWT-Food Science and Technology, 153*, Article 112445. https://doi.org/10.1016/j.lwt.2021.112445

Wang, T., Sun, X., Raddatz, J., & Chen, G. (2013). Effects of microfluidization on microstructure and physicochemical properties of corn bran. *Journal of Cereal Science, 58*, 355–361. https://doi.org/10.1016/j.jcs.2013.07.003

Xiang, A., Li, W., Zhao, Y., Ju, H., Xu, S., Zhao, S., Yue, T., & Yuan, Y. (2022). Purification, characterization and antioxidant activity of selenium-containing polysaccharides from pennycress (*Thlaspi arvense* L.). *Carbohydrate Research, 512*, Article 108498. https://doi.org/10.1016/j.carres.2021.108498

Xiao, D., Li, T., Huang, X., Zhu, K., Li, Z., Dong, Y., … Huang, J. (2023). Advances in the study of selenium-enriched probiotics: From the inorganic se into se nanoparticles. *Molecular Nutrition & Food Research, 67*, 2300432. https://doi.org/10.1002/mnfr.202300432

Xiong, X., Cao, X., Zeng, Q., Yang, X., Wang, Y., Zhang, R., Huang, F., Dong, L., Zhang, M., & Su, D. (2021). Effects of heat pump drying and superfine grinding on the composition of bound phenolics, morphology and microstructure of lychee juice by-products. *LWT-Food Science and Technology, 144*, Article 111206. https://doi.org/10.1016/j.lwt.2021.111206

Yu, J., Wang, G., Wang, X., Xu, Y., Chen, S., Wang, X., & Jiang, L. (2018). Improving the freeze-thaw stability of soy protein emulsions via combing limited hydrolysis and Maillard-induced glycation. *LWT-Food Science and Technology, 91*, 63–69. https://doi.org/10.1016/j.lwt.2018.01.031

Zahedi, S. M., Hosseini, M. S., Daneshvar, H. M. N., & Teixeira da Silva, J. A. (2019). Foliar application of selenium and nano-selenium affects pomegranate (*Punica*

granatum cv. *Malase Saveh*) fruit yield and quality. *South African Journal of Botany, 124*, 350–358. https://doi.org/10.1016/j.sajb.2019.05.019

Zhang, J., Dong, Y., Nisar, T., Fang, Z., & Guo, Y. (2020). Effect of superfine-grinding on the physicochemical and antioxidant properties of *Lycium ruthenicum* Murray powders. *Powder Technology, 372*, 68–75. https://doi.org/10.1016/j.powtec.2020.05.097

Zhang, L., Xu, H., & Li, S. (2009). Effects of micronization on properties of *Chaenomeles sinensis* (Thouin) Koehne fruit powder. *Innovative Food Science & Emerging Technologies, 10*, 633–637. https://doi.org/10.1016/j.ifset.2009.05.010

Zhang, M., Wang, F., Liu, R., Tang, X. L., Zhang, Q., & Zhang, Z. S. (2014). Effects of superfine grinding on physicochemical and antioxidant properties of *Lycium barbarum* polysaccharides. *LWT-Food Science and Technology, 58*, 594–601. https://doi.org/10.1016/j.lwt.2014.04.020

Zhang, Y., Li, R. D., Shang, G. N., Zhu, H., Mahmood, N., & Liu, Y. H. (2021). Mechanical grinding alters the physicochemical, structural, and functional properties of tobacco (*Nicotiana tabacum* L.) leaf powders. *Industrial Crops and Products, 173*, Article 114149. https://doi.org/10.1016/j.indcrop.2021.114149

Zhang, Z., Lv, G., He, W., Shi, L., Pan, H., & Fan, L. (2013). Effects of extraction methods on the antioxidant activities of polysaccharides obtained from *Flammulina velutipes*. *Carbohydrate Polymers, 98*, 1524–1531. https://doi.org/10.1016/j.carbpol.2013.07.052

Zhao, X., Du, F., Zhu, Q., Qiu, D., & Yin, W. (2010). Effect of superfine pulverization on properties of *Astragalus membranaceus* powder. *Powder Technology, 203*, 620–625. https://doi.org/10.1016/j.powtec.2010.06.029

Zhao, X. Y., Liu, H. K., Zhang, X. W., & Ao, Q. (2018). Effect of pressure grinding technology on the physicochemical and antioxidant properties of *Tremella aurantialba* powder. *Journal of Food Processing and Preservation, 42*. https://doi.org/10.1111/jfpp.13833

Zhao, X. Y., Zhu, H. T., Chen, J., & Ao, Q. (2015). FTIR, XRD and SEM analysis of ginger powders with different size. *Food Processing and Preservation, 39*, 2017–2026. https://doi.org/10.1111/jfpp.12442

Zhu, L., Yu, B., Chen, H., Yu, J., Yan, H., Luo, Y., He, J., Huang, Z., Zheng, P., Miao, X., Luo, J., & Chen, D. (2022). Comparisons of the micronization, steam explosion, and gamma irradiation treatment on chemical composition, structure, physicochemical properties, and in vitro digestibility of dietary fiber from soybean hulls. *Food Chemistry, 366*, Article 130618. https://doi.org/10.1016/j.foodchem.2021.130618